Bulletin of the
Seismological Society of America

Vol. 70 December No. 6

DETERMINATION OF SOURCE PARAMETERS OF MID-PLATE EARTHQUAKES FROM THE WAVEFORMS OF BODY WAVES

By Hsui-Lin Liu and Hiroo Kanamori

ABSTRACT

The source parameters and stress drops of five mid-plate earthquakes were determined by matching the synthetic and observed far-field *P* waveforms in the time domain. The stress drops estimated from these mid-plate events are on the order of a hundred to a few hundred bars. These values are significantly higher than those for interplate (30 bars) and intraplate (100 bars) earthquakes which occurred near the plate boundaries. The difference of the earthquake stress levels between mid-plate and plate boundary events may suggest a lateral variation of stress level in the lithosphere and provide important constraints on the driving mechanism of plate motion.

Introduction

Sykes and Sbar (1973, 1974) investigated the focal mechanisms of about 80 intraplate earthquakes and indicated that the interior of many lithospheric plates are characterized by large horizontal compressive stresses. The general features of this group of earthquakes are the relatively infrequent occurrence, diverse spatial distribution, and high frequency content of seismic waves (Sykes and Sbar, 1973). They also pointed out that these stresses seem to be related to the driving mechanism of plate tectonics. However, the details of the source processes of intraplate earthquakes are not well understood. A variety of possible models have been proposed to explain the driving mechanisms of plate motions on the basis of intraplate stress orientation (Sykes and Sbar, 1974; Richardson *et al.*, 1976; Richardson, 1978). A more quantitative understanding of source processes of these events is important for evaluating these models.

The present paper is mainly concerned with the source processes of mid-plate earthquakes, which are intraplate events occurring far away from plate boundaries. The empirical relationship between the fault area and the seismic moment noted by Kanamori and Anderson (1975) indicates that the intraplate earthquakes are characterized by higher stress drops than interplate earthquakes. Furthermore, anomalous m_b versus M_S relation for the earthquakes in the Eurasian interior has been interpreted as the relative enrichment of short-period waves, which may result from short rupture duration or small source dimension (Tatham *et al.*, 1976; Kim and Nuttli, 1977). It has also been speculated that these anomalous events may be related to high stress concentrations or the stress fields responsible for new fault creation. These findings motivated the present study in which we attempt to obtain more accurate source parameters by matching the synthetic and observed far-field

P waveforms in time domain. Since most mid-plate earthquakes are shallow events, the effect of the free surface on the waveform is very significant. The advantage of the time domain method is that the free surface effect can be accounted for in a straightforward way (Langston, 1978).

Mid-plate Earthquakes

The five earthquakes we used in this study are listed in Table 1 and their locations are shown in Figure 1. We chose these earthquakes from the intraplate events listed in Sykes and Sbar (1974) on the basis of the quality of the body wave signal. The body waves from these events are simple enough to allow us to study more details of the source process by using body wave synthetics.

The 16 April 1965 event (no. 1) is located in Alaska. This is the largest event (m_b = 5.8) in this area since 1962. The fault plane solution of this earthquake which was determined by the first motion study (Sykes and Sbar, 1974) has a normal fault geometry with strike = 305°, dip = 66°, and slip angle = −85°. As will be shown later, the synthetic seismograms computed for this mechanism fit the observed waveforms quite well.

The 4 September 1963 earthquake (no. 2) which occurred in the Baffin Island area is a normal fault event dominated by dip-slip motion. The fault plane solution is well constrained by the first motions with strike = 93°, dip = 70°, and slip angle = −94° (Sykes, 1970). This event is classified as a continental margin earthquake, with the tensional deviatoric stress oriented nearly perpendicular to the continental margin (Sykes and Sbar, 1974). Sykes and Sbar (1974) suggested that the stress field associated with the continental margin may be related to the slow cooling and subsidence of oceanic crust near the margin area. Recently, Stein *et al.* (1979, in preparation) proposed that the regional stress around this passive margin area of Eastern North America can be interpreted as a deglaciation effect.

Both the 23 October 1964 (no. 3) and the 30 September 1971 (no. 4) events are located in the Atlantic Ocean as indicated in Figure 1. The focal mechanisms of both events are not well constrained by the first motion study. Sykes and Sbar (1974) concluded that all the focal mechanisms of the events which are located far away from the ridges in the Atlantic Ocean are characterized by thrust faulting. They also suggested that the directions of the maximum compressive stress seem to be perpendicular to the isochrons in the oceanic lithosphere. However, as will be shown later, the directions of maximum compressive stresses of events nos. 3 and 4 are more parallel than perpendicular to the isochrons. It is thus difficult to explain the origin of stress at this point to be a cooling process in oceanic lithosphere.

The 24 March 1970 earthquake (no. 5) occurred in Lake MacKay, Western Australia. Since all the stations with available records are in the same quadrant of the focal sphere, the fault plane solution is mainly determined by the *S*-wave polarization angles (Fitch *et al.*, 1973). This focal mechanism has strike = 352°, dip = 52°, and slip angle = 125°. The direction of the maximum compressive stress for this event is consistent with the general stress trend in Australia, with the maximum stress oriented in the direction from E–W to NW–SE. The currently accepted explanation of this regional stress is that they result from the collision of the Indian Plate with Tibet along the Himalayas (Fitch *et al.*, 1973).

Body Wave Analysis

All the events studied here have simple far-field waveforms which are amenable to time domain body-wave analysis. The method applied in this paper has been

TABLE 1

EARTHQUAKES AND STATIONS USED IN THIS STUDY

Event No.	Date	Origin Time (h m s)	Location	m_b	Stations	Distance (°)	Azimuth (°)
1	16 April 1965	23 22 18	64.7°N 160.1°W (Back-arc area, North American Plate)	5.8 (USGS)	ALQ	43.66	106
					ANP	62.53	271
					AQU	73.16	5.0
					ATU	77.66	356.9
					BAG	70.68	267.0
					BEC	63.45	70.3
					BKS	34.86	121.8
					CAR	82.0	83.0
					CHG	77.76	287.9
					DAL	49.47	98.3
					DUG	36.51	108.9
					GHD	36.87	34.7
					GOL	40.01	101.6
					GSC	39.16	117.4
					HKC	68.21	276.0
					LON	27.48	112.0
					MAL	78.12	12.7
					NDI	76.87	310.6
					POO	87.36	310.0
					PTO	72.18	22.0
					QUE	78.56	319.7
					SHL	74.48	296.9
					STU	66.58	8.0
					TUC	44.2	113.0
2	4 September 1963	13 32 8.0	71.31°N 73.02°W (Continental margin, North American Plate)	5.9	ALQ	40.47	224.2
					AQU	49.44	76.9
					BKS	41.82	244.0
					COP	37.39	68.4
					COR	35.95	249.4
					DAL	40.58	211.4
					GSC	42.69	236.6
					KEV	29.78	43.6
					LUB	40.8	218.1
					NDI	78.2	26.5
3	23 October 1964	01 56 3.25	19.8°N 56.0°W (Atlantic Ocean, Central American Plate)	6.4 (USGS)	ALQ	46.80	300.0
					COP	61.80	37.0
					COR	60.24	311.0
					LPB	37.98	199.0
					LUB	42.79	298.0
					TUC	50.3	296.0
					STU	59.15	44.0
					WIN	82.94	117.0
4	30 September 1971	21 24 8.0	0.4°S 4.7°W (Atlantic Ocean, African Plate)	6.0 (NEIC)	ESK	55.6	1.0
					GRM	44.07	141.0
					HLW	45.82	46.0
					IST	51.48	33.0
					KOD	82.56	80.0
					LPS	84.56	284.0
					SHI	62.29	56.0
					STU	50.52	12.0
					TRN	57.25	283.0
					VAL	52.39	356.0

TABLE 1—*Continued*

Event No.	Date	Origin Time (h m s)	Location	m_b	Stations	Distance (°)	Azimuth (°)
5	24 March 1970	10 35 12.9	21.9°S 126.6°E (Continent, Indian-Australian Plate)	6.2	BAG	38.71	351.0
					BUL	89.65	248.0
					GRM	76.9	183.0
					HKC	45.76	344.0
					HNR	34.34	74.0
					NAI	89.3	269.0
					NDI	69.41	315.0
					PRE	87.79	243.0
					RAB	30.46	58.0
					SHL	58.14	323.0
					SNG	38.5	316.0

used for source studies of various events (Helmberger, 1974; Langston, 1975; Kanamori and Stewart, 1976; Chung and Kanamori, 1976). Basically, we model the far-field seismograms by convolving the sum of various body wave rays (e.g., *P*, *pP*, and

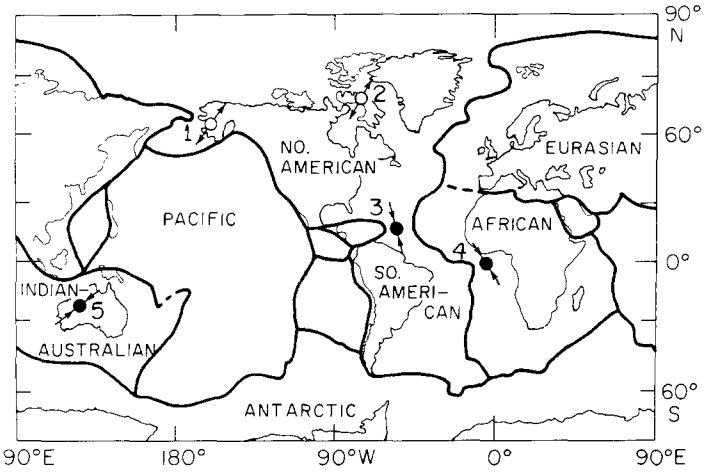

FIG. 1. Global map indicating tectonic plates and locations of earthquakes used in this study. The event numbers are the same as listed in Table 1. Solid dots are thrust faults and open circles are normal faults. The arrows show the directions of maximum stress.

sP) with source time history, earth attenuation, crustal structure, and instrument response. The displacement $U_c(t)$ of *P* or *S* waves can be represented by

$$U_c(t) = \frac{M_0}{4\pi\rho_h V_{c,h}^3} \frac{g(\Delta, h)}{a} R_{\theta\phi}^c \cdot S(t - T_0^c) * Q\left(t, \frac{T_0^c}{Q_{av}^c}\right) * C(t) * I(t)$$

where

M_0 = seismic moment
h = source depth
ρ_h = the density at the source
$V_{c,h}$ = the wave velocity at the source
c = P or S waves
$g(\Delta, h)$ = the geometrical spreading factor
a = Earth's radius

$R^c_{\theta\phi}$ = the radiation pattern
S = far-field source time function
$T_0{}^c$ = travel time
$Q\left(t, \frac{T_0{}^c}{Q^c_{av}}\right)$ = Q function (Carpenter, 1966)
Q^c_{av} = the average value of Q along the ray path
$C(t)$ = the crust filter
$I(t)$ = the instrument response.

To avoid the complexity in the travel-time curves caused by heterogeneity of the upper mantle and the core-mantle boundary, we use stations with epicentral distances from 30° to about 85°. In the present study, we use a half-space to represent the structure. By matching the synthetics with the observed seismograms, we can obtain source parameters, such as fault orientation, source depth, source time duration, and seismic moment. In principle, the focal mechanism determines the polarity and the relative amplitude of each phase (P, pP, sP for P waves and S, sS for SH waves); the source time duration controls the pulse width, and the depth

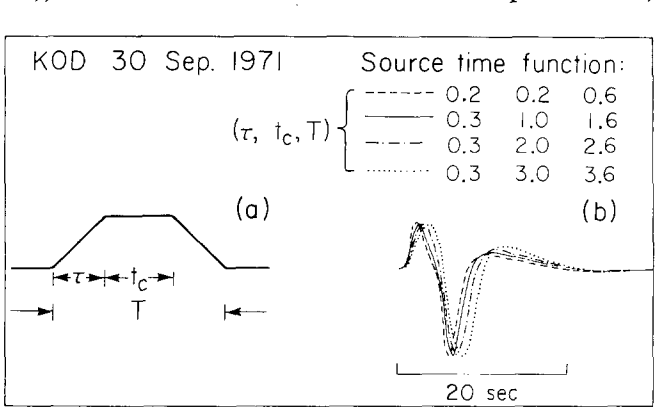

FIG. 2. (a) Trapezoid function used for the synthetics. τ is the rise time, $(\tau + t_c)$ is the rupture time, and T is the total duration. (b) The P synthetic waveforms for different source time functions.

determines the time-lag between different phases. For actual calculations, we use $\frac{T_0}{Q^c_{av}} = 1$ for P waves and $\frac{T_0}{Q^c_{av}} = 4$ for S waves. The source time function we used for the synthetics is a symmetric trapezoidal function as shown in Figure 2a, where τ is the rise time, and $(t_c + \tau)$ is the rupture duration. The change of the synthetic waveforms due to the change of total source time duration T is demonstrated in Figure 2b with the other source parameters fixed. We can resolve the total duration T up to ±1 sec. However, for a fixed total duration, there are no resolvable differences for the various combinations of τ and t_c. Since there is no available aftershock information, we estimated the fault area by the following method. If we assume that the fault geometry is circular, and the effective stress is equal to the stress drop, then the radius of the circular fault, γ, is proportional to the source time duration, T, and is given by the following relation (Geller, 1976; Ebel *et al.*, 1978)

$$\gamma = \frac{28\pi\beta T}{64 + 7\pi(5 + 4 \sin \delta)},$$

where β is the shear velocity, and δ is the angle between the normal to the fault plane and the ray direction.

The comparison of the observed seismograms and synthetics for the 1965 event (no. 1) is shown in Figure 3. The source mechanism determined by first motion study (strike = 305°, dip = 66°, slip angle = −85°; Sykes and Sbar, 1974) fits the observed data quite well with a depth of 12 km and a source time duration of 3.4 sec. Those stations with azimuths from about 90° to 120° (DAL, GOL, LON, ALQ, DUG, TUC, and GSC) all have a strong third swing around 10 sec after the onset which cannot be modeled by these source parameters. This third swing might be caused by the receiver structure and/or the asymmetric radiation at the source. The seismic moment estimated from the amplitude ratio between the observed and synthetic seismograms is 1.3×10^{25} dyne-cm, and the fault areas estimated with the circular fault assumption are 52 and 72 km^2, respectively, for the two fault planes. The corresponding stress drops are 51 and 83 bars.

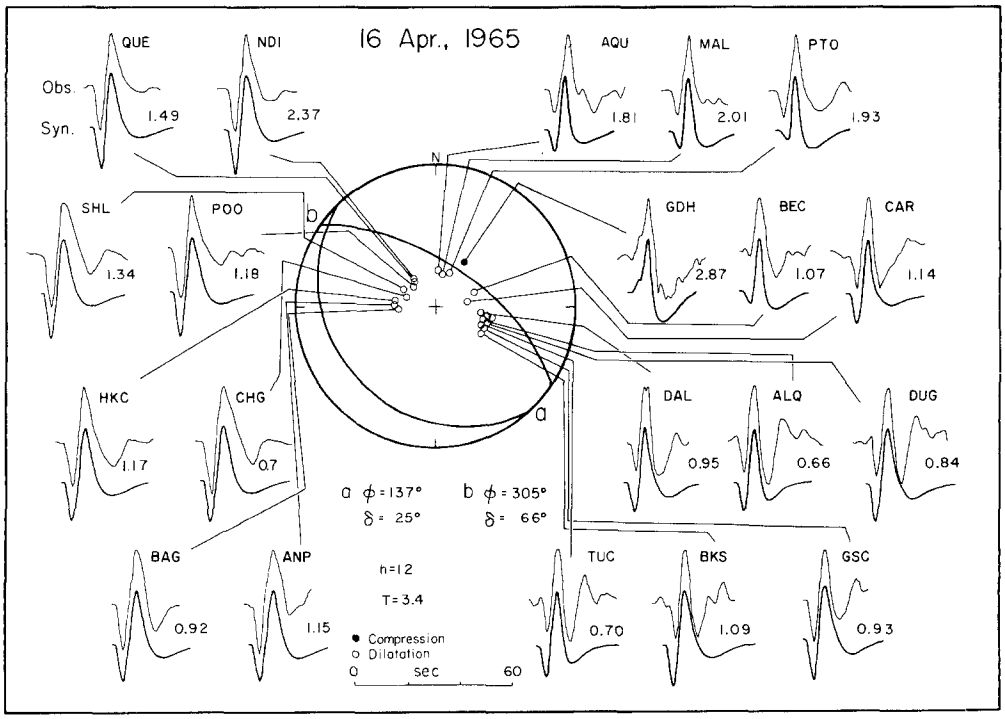

FIG. 3. Comparison of observed (upper) and synthetic (lower) *P* waves of 16 April 1965 earthquake. The numbers are the seismic moments estimated from each station, with units of 10^{25} dyne-cm. Synthetics are computed for a point source in a half-space with a depth of 12 km and a trapezoidal far-field time function with a duration of 3.4 sec. Only stations for which we generated synthetics are plotted on the focal sphere.

The focal mechanism (strike = 98°, dip = 66°, slip angle = −103°) of the 1963 event (no. 2) determined by this study is slightly different from the solution obtained by the first motion study. Ten synthetic seismograms which are shown in Figure 4 suggest that the best fit is obtained for a depth of 7 km with a source time duration of 2.5 sec. Stations are chosen to give optimal azimuthal coverage. The seismic moment is 1.7×10^{25} dyne-cm, and the fault area is 28 to 38 km^2, and the stress drop is 171 to 274 bars.

Both the synthetic and observed seismograms of the 1964 event (no. 3) are shown in Figure 5. The synthetics computed for the source mechanism (strike = 296°, dip = 66°, slip angle = 158°) fit the observed seismograms well with a depth of 23 km and a source time duration of 2.5 sec. The source depth is mainly determined by the

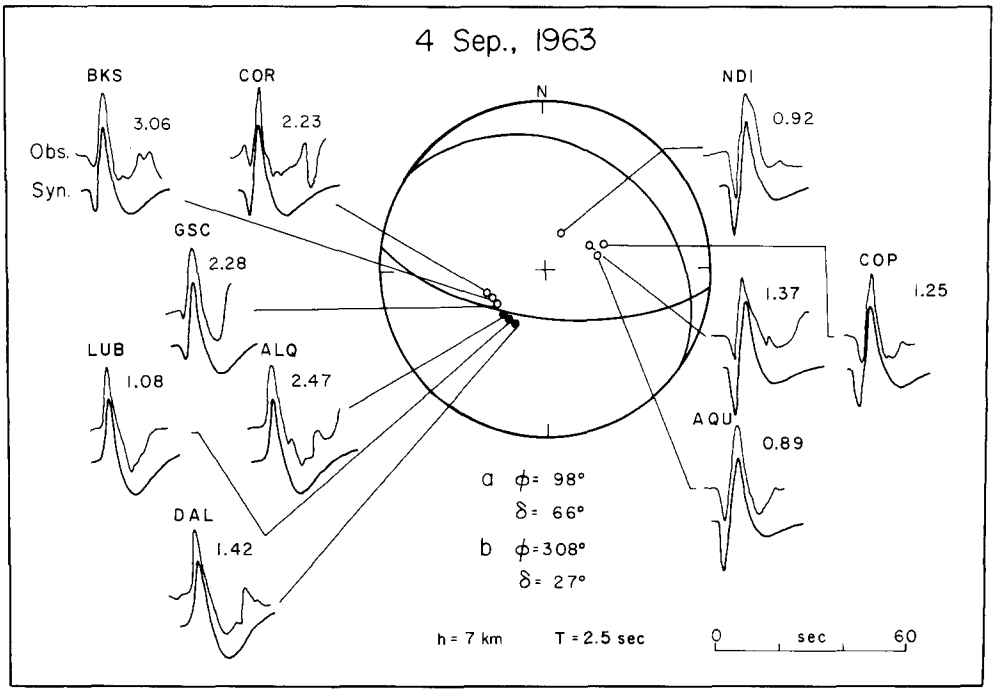

FIG. 4. Observed and synthetic seismograms of P waves for the 4 September 1963 event. Seismic moment estimated for each station is shown by the number with 10^{25} dyne-cm unit scale. The letters a and b here refer to the two fault plane solutions, h is the source depth, and T is the source time duration.

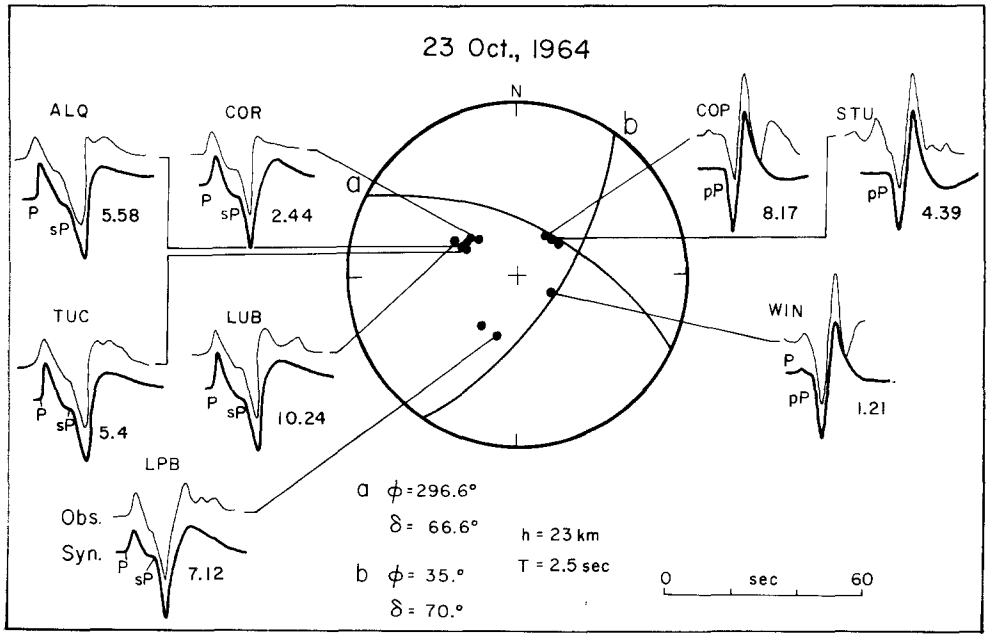

FIG. 5. Comparison of observed and synthetic seismograms for the 23 October 1964 event. The synthetics are constructed for the source geometry indicated by a and b with a source depth of 23 km and source time duration of 2.5 sec.

arrival time of the free surface reflected phases (pP or sP) which show very clear arrivals in the records as indicated in Figure 5. The seismic moment is 6.2×10^{25} dyne-cm, and the fault area is from 28 to 29 km^2, and the stress drop is 880 to 907 bars.

The 1971 event (no. 4) is another oceanic event besides the 1964 event (no. 3) in this study. The source parameters determined are: strike = 72°, dip = 60°, slip angle = 60°; source depth = 13 km; and source time duration = 1.6 sec, as shown in Figure 6. The source mechanism determined from the *P*-wave analysis is used to generate

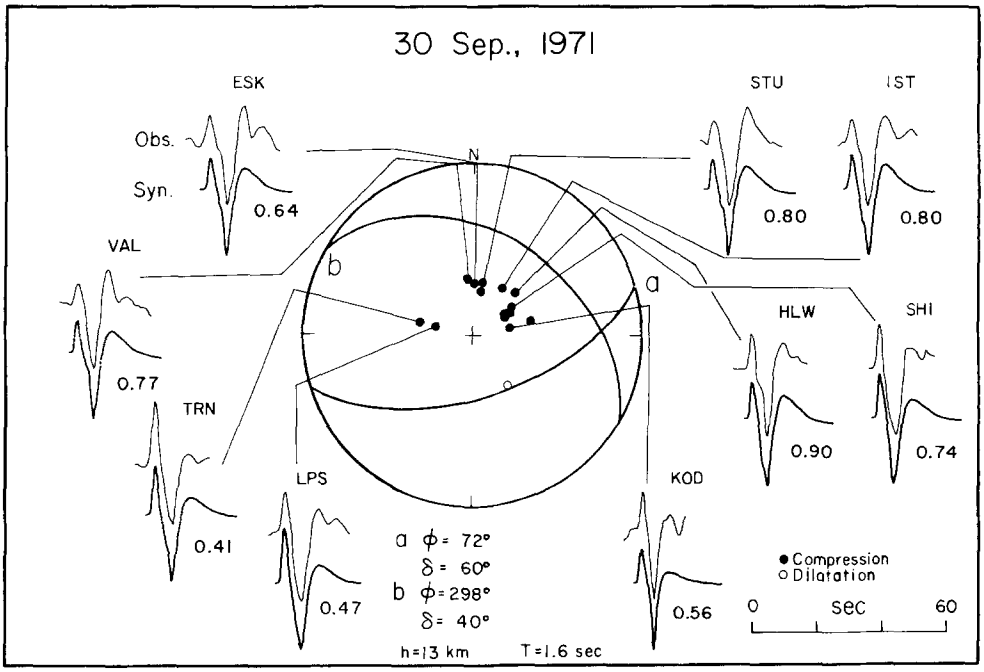

FIG. 6. Observed and synthetic seismograms of the 30 September 1971 earthquake. The numbers are the seismic moments for different stations with a unit of 10^{25} dyne-cm.

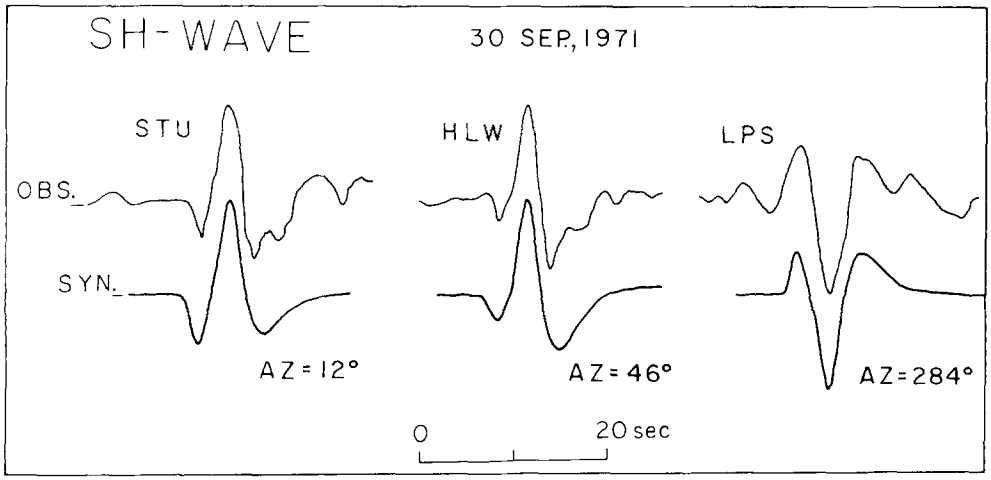

FIG. 7. Comparison of observed and synthetic *SH* waveforms for the stations STU, HLW, and LPS of the 30 September 1971 earthquake. The source parameters are the same as those used to compute synthetic *P* waves.

the *SH* synthetics. As is shown in Figure 7, the observed *SH* waveforms at STU, HLW, and LPS can be matched very well by the synthetics. Since the estimated source depth may be somewhat structure-dependent, we also tested the effect of a water layer for this event. A 2.5-km water layer with 1-km sedimentary layer over

a half-space is used to represent the oceanic source structure (Harkrider and Anderson, 1966). Figure 8 shows the comparison between the observed seismograms, half-space synthetics, and water-layer synthetics for 5 stations: IST (azimuth = 33°), SHI (azimuth = 56°), KOD (azimuth = 80°), TRN (azimuth = 283°), and VAL (azimuth = 356°). It seems that the multiples generated by water and sedimentary layers at this depth arrive at least 10 sec after the first arrival. The half-space is therefore a reasonably good model to explain the first part of the body waveform.

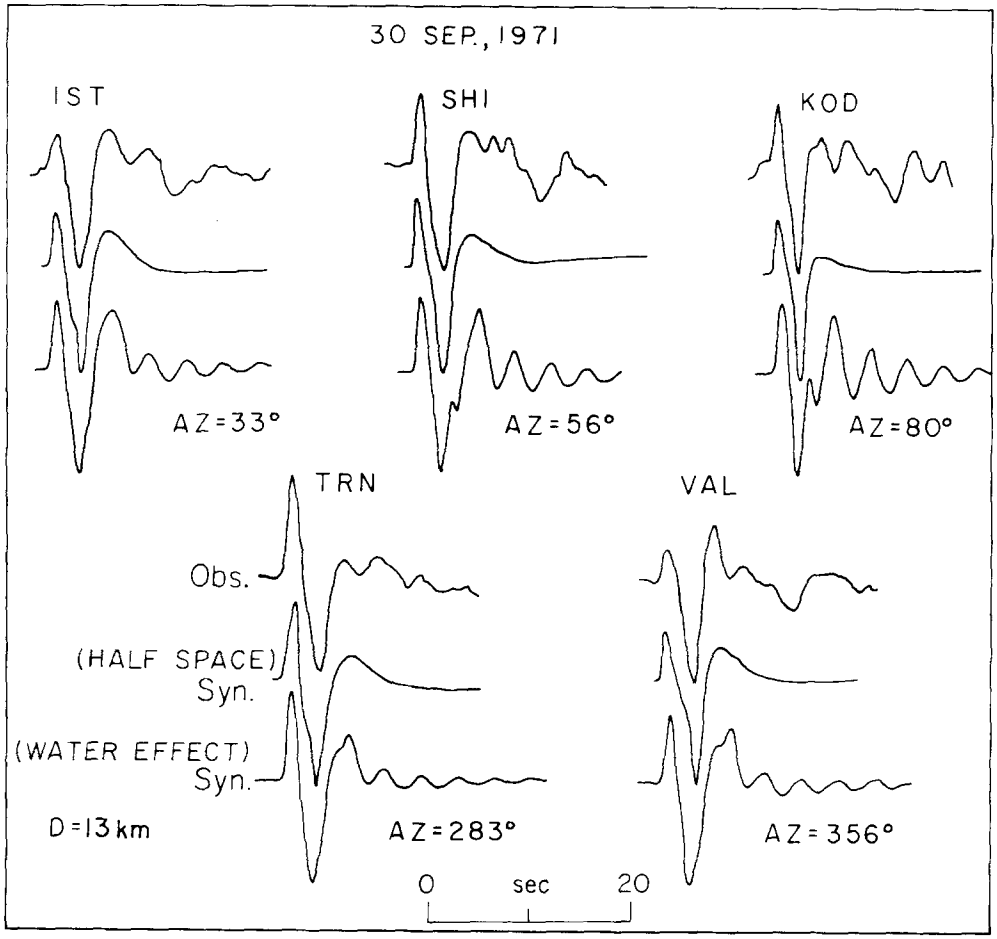

FIGURE 8. *P*-wave synthetics for both half-space and water-layer structures. The structure we used to compute the water effect is listed as follows

Layer	v_p(km/sec)	v_s(km/sec)	Density	Thickness (km)
1	1.52	0.01	1.03	2.5
2	2.10	1.00	2.10	1.0
3	6.40	3.7	3.09	half-space.

The focal mechanism is the same as in Figure 5.

The seismic moment estimated from the *P* waves is 0.7×10^{25} dyne-cm, and the fault area is from 11 to 12 km^2, and the stress drop is 370 to 425 bars.

Figure 9 shows the comparison between observed and synthetic seismograms for the 1970 event. The source parameters are: strike = 305°, dip = 56°, slip angle = 112° with a source depth of 12 km and source time duration of 2.5 sec. The seismic moment is determined to be 1.4×10^{25} dyne-cm. The fault area is from 29 to 36 km^2, and the stress drop is from 149 to 204 bars.

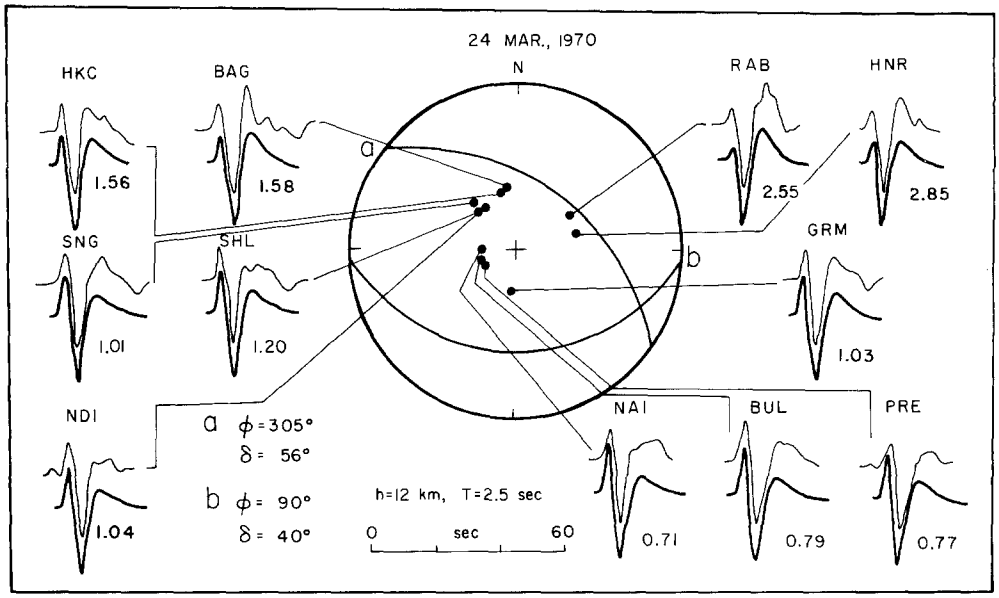

FIG. 9. The comparison of observed and synthetic seismograms of the 24 March 1970 event. The synthetics are constructed for the source mechanism indicated by a and b. The source depth is 12 km, and the source time duration is 2.5 sec. The numbers are seismic moments with units of 10^{25} dyne-cm.

COMPARISON AND DISCUSSION

The source parameters determined in this study are listed in Table 2 for comparison. The 1965 event (no. 1) which occurred in the Alaskan back-arc area shows the lowest stress drop of the five earthquakes studied. Somewhat higher stress drops were determined for events nos. 2 (Baffin Island) and 5 (Western Australia). The 1964 (no. 3) and 1971 (no. 4) events, both located in the Atlantic Ocean, yielded the highest stress drops for this group. Figure 10 shows the log M_0 (seismic moment) versus log S (fault area) plot and the comparison of these events with the average trend. Kanamori and Anderson (1975) concluded that a constant average stress drop of about 60 bars represents the linear relation between log S and log M_0 for large earthquakes ($M_S \geqq 6$). The magnitude (m_b) of earthquakes in this study ranges from 5.8 to 6.4, but only the 1965 event has a stress drop close to this average level; the other events have higher stress drops.

Since the fault area could not be estimated directly, the values of the stress drops are somewhat uncertain. In order to compare the mid-plate earthquakes with other events in terms of parameters which can be determined directly from observations, we plot the seismic moment against the source time duration in Figure 11. Both of these parameters were determined directly by matching the synthetics and observed waveforms. The solid dots with the numbers are the events studied here. The circles represent the data for events taken from Helmberger and Johnson (1977). Although these events were studied by different investigators (Helmberger and Johnson, 1977; Langston and Butler, 1976; Langston, 1976; Burdick and Mellman, 1976), the technique used to determine the source time duration and the seismic moment is the same. The time duration plotted in Figure 11 is defined according to Helmberger and Johnson (1977). The thin solid and dashed lines represent constant stress drop lines for two different source models, one by Brune (1970) and the other by Madariaga (1976). Although the absolute value of the stress drop is model-depen-

TABLE 2

SOURCE PARAMETERS

Event No.	Date	m_b	First Motion Study			This Study			Moment (M_0) ($\times 10^{25}$ dyne-cm)	Depth (h) (km)	Source Time (sec)	Fault Area (km^2)	Stress Drop (bars)
			Strike (°)	Dip Angle (°)	Slip Angle (°)	Strike (°)	Dip Angle (°)	Slip Angle (°)					
1	16 April 1965	5.8	305*	66	85	305	66	−85	1.3	12.0	3.4	52.0, 72.0	51, 83
2	4 September 1963	5.9	93†	70	−94	98	66	−103	1.7	7.0	2.5	28.0, 38.0	171, 274
3	23 October 1964	6.4	284*	52	137	296	66	158	6.2	23.0	2.5	28.0, 29.0	880, 907
4	30 September 1971	6.0	72*	60	117	72	60	60	0.7	13.0	1.6	11.0, 12.0	370, 425
5	24 March 1970	6.2	352‡	52	125	305	56	112	1.4	12.0	2.5	29.0, 36.0	149, 204

* Source: Sykes and Sbar, 1974.
† Source: Sykes, 1970.
‡ Source: Fitch, 1973.

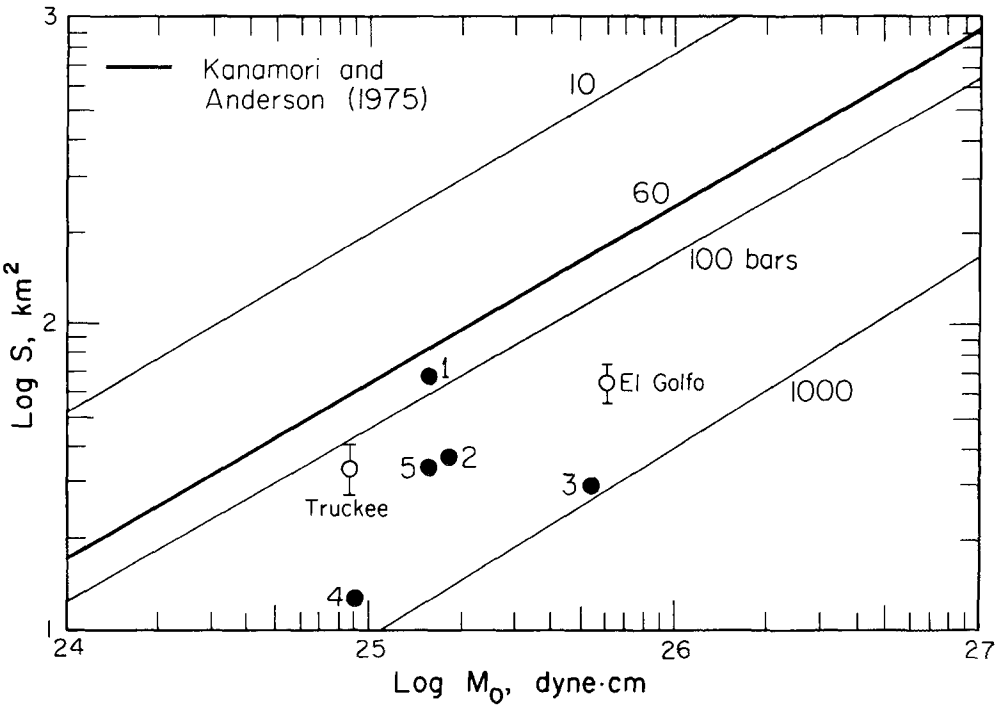

FIG. 10. Log S versus log M_0 plot for the mid-plate events in this study (the fault area plotted here is the average value for both fault planes) and the empirical relation for large earthquakes ($M_S \gtrsim 6$).

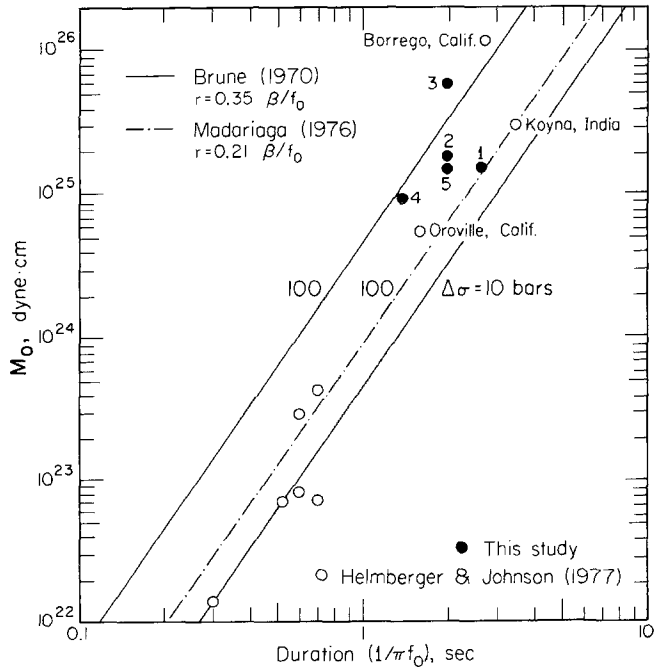

FIG. 11. Moment versus duration plot for the mid-plate events of this study and some plate boundary or plate boundary-associated events.

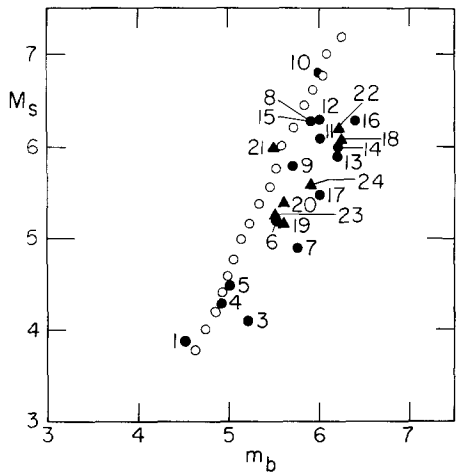

FIG. 12. M_S versus m_b plot for mid-plate events (solid dots) and worldwide average data (circles). The data and references are listed in Table 3.

TABLE 3

LISTING OF m_b AND M_S FOR MID-PLATE EARTHQUAKES

No.	Date*	m_b†	M_S†	Location
1	14 May 1964	4.5	3.9‡	65.3N, 86.5W; North American Plate
2	21 January 1972	4.2		71.4N, 74.7W; North American Plate
3	21 October 1965	5.2	4.1‡	37.6N, 90.9W; North American Plate
4	2 December 1970	4.9	4.3‡	68.4N, 67.4W; North American Plate
5	2 October 1971	5.0	4.5‡	64.4N, 86.5W; North American Plate
6	9 November 1968	5.5‡	5.2‡	38.0N, 88.5W; North American Plate
7	25 November 1965	5.75§	4.9‡	17.1S, 100.2W; Nazca Plate
8	29 September 1969	5.9	6.3	33.2S, 19.3E; African Plate
9	20 October 1972	5.7	5.8	20.6N, 29.7W; Atlantic Ocean
10	14 October 1968	6.0	6.8	31.7S, 117.0E; Australian Plate
11	26 April 1973	6.0	6.1	20.2N, 155.2W; Pacific Ocean
12	10 December 1967	6.0	6.3‡	17.6N, 73.8E; Indian-Australian Plate
13	24 March 1970**	6.2	5.9	22.1S, 126.6E; Indian-Australian Plate
14	9 May 1971	6.2	6.0	39.8S, 104.9W; Antarctic Plate
15	10 October 1970	5.9	6.3	3.6S, 86.2E; Indian-Australian Plate
16	23 October 1964**	6.4	6.3	19.8N, 56.1W; Atlantic Ocean
17	30 September 1971**	6.0	5.5	0.4S, 4.7W; Atlantic Ocean
18	12 September 1965††	6.2	6.0	6.5S, 70.8E; Indian-Australian Plate
19	11 November 1967	5.6	5.2	6.0S, 71.3E; Indian-Australian Plate
20	2 March 1968	5.6	5.4	6.1S, 71.4E; Indian-Australian Plate
21	25 May 1964	5.5	6.0	9.1S, 88.9E; Indian-Australian Plate
22	25 June 1974	6.2	6.2	26.1S, 84.3E; Indian-Australian Plate
23	28 April 1965	5.5	5.2	44.8N, 174.6E; Pacific Plate
24	7 October 1965	5.9	5.6	12.5N, 114.5E; Eurasian Plate (South China Sea)

* The mid-plate earthquakes nos. 1–16 are taken from Richardson and Solomon (1977).

† The m_b and M_S data are taken from USCGS except as indicated. (The data are the same as those reported by PDE except m_b = 5.3 for event no. 6).

‡ Data taken from Richardson and Solomon (1977).

§ Source: Mendiguren (1971).

** These three events are studied in this paper.

†† The magnitude data of earthquakes nos. 18–24 are provided by Stein [Stein, 1978; Stein and Okal, 1978; Stein, 1979 (in preparation); Wang *et al.*, 1979].

dent, the mid-plate events studied here seem to have higher stress drops than any other events except the Borrego Mountain earthquake.

Another way to infer the difference in the stress level is to compare the frequency content of earthquakes. Since the body wave magnitude, m_b, is proportional to the amplitude of about 1-sec waves and the surface wave magnitude, M_S, is proportional to the amplitude of 20-sec waves, the ratio of these two may indicate the stress level at the source (Archambeau, 1978). Although the absolute value of stress drop cannot be determined unambiguously from the M_S/m_b ratio, the events with a larger m_b value for a given M_S would indicate a higher stress drop. Here we plot M_S versus m_b for the mid-plate earthquakes in Figure 12. The circles represent the average (with error of ± 0.25 m_b) $M_S - m_b$ relation obtained from worldwide shallow (depth less than 50 km) earthquakes for the years 1973 to 1975 determined by Noguchi and Abe (1977). The data are taken rom the PDE monthly listings. The solid dots (nos. 1 to 16) are the $M_S - m_b$ plot for the mid-plate events taken from Richardson and Solomon (1977). The solid triangles are the magnitude data of the intraplate earthquakes taken from Stein (1978), Stein and Okal (1978), Stein (1979, in preparation), and Wang *et al.* (1979). The values of m_b and M_S and the locations of the events are listed in Table 3. Although the number of mid-plate earthquakes is very limited, the mid-plate events seem to have larger m_b than the average events with the same M_S, substantiating the conclusion obtained from the analysis of body waveforms.

Conclusions

The source parameters and stress drops of five mid-point earthquakes were determined by matching the synthetic and observed P waveforms in the time domain. The location of these events include the North American Plate (back-arc area and continental margin), the African Plate (ocean area), the South American Plate (ocean), and the Australian Plate (continent). The seismic moment estimated for these events ranges from 0.9 to 6.1×10^{25} dyne-cm and source time durations from 1.6 to 3.4 sec. Based on the assumption of circular faulting, the stress drops determined for these events are on the order of a hundred to a few hundred bars. Except for event no. 1, which is located in the back-arc area of Alaska, the studied events have higher stress drops than the average value (60 bars) or worldwide large earthquakes. The seismic moment versus source time duration and M_S versus m_b plots also suggest that mid-plate earthquakes appear to have relatively high stress drops. We need more data to substantiate this conclusion, but the indication of a higher stress level for mid-plate earthquakes, especially oceanic events, may provide significant constraints on tectonic stress models.

Acknowledgments

We would like to thank Wai Ying Chung for assistance in the early phases of this study, Tom Heaton for critically reading the manuscript, John Cipar for useful discussions, and Seth Stein for comments on the manuscript. This research was supported by the Earth Sciences Section, National Science Foundation Grant EAR 78-11973.

References

Archambeau, C. B. (1978). Estimation of non-hydrostatic stress in the earth by seismic methods: lithospheric stress levels along Pacific and Nazca Plate subduction zones, *U.S. Geol Surv., Open-File Rept. 78-943*, 47–138.

Brune, J. N. (1970). Tectonic stress and the spectra of seismic shear waves from earthquakes, *J. Geophys. Res.* **75**, 4977–5009.

Burdick, L. J. and G. R. Mellman (1976). Inversion of the body waves from the Borrego Mountain

earthquake to the source mechanism, *Bull. Seism. Soc. Am.* **66,** 1485–1499.
Carpenter, E. W. (1966). Absorption of elastic waves—An operator for a constant Q mechanism, AWRE Report)-43/66, London, Her Majesty's Stationary Office, 16 pp.
Chung, W.-Y. and H. Kanamori (1976). Source process and tectonic implications of the Spanish deep-focus earthquake of March 29, 1954, *Phys. Earth Planet. Interiors* **13,** 85–96.
Ebel, J. E., L. J. Burdick, and G. S. Stewart (1978). The source mechanism of the August 7, 1966 El Golfo earthquake, *Bull. Seism. Soc. Am.* **68,** 1281–1292.
Fitch, T. J., M. H. Worthington, and L. B. Everingham (1973). Mechanisms of Australian earthquakes and contemporary stress in the Indian Ocean plate, *Earth Planet. Sci. Letters* **18,** 345–356.
Geller, R. J. (1976). Scaling relations for earthquake source parameters and magnitudes, *Bull. Seism. Soc. Am.* **66,** 1501–1523.
Harkrider, D. G. and D. L. Anderson (1966). Surface wave energy from point sources in plane layered earth models, *J. Geophys. Res.* **71,** 2967–2980.
Helmberger, D. V. (1974). Generalized ray theory for shear dislocations, *Bull. Seism. Soc. Am.* **62,** 561–589.
Helmberger, D. V. and L. R. Johnson (1977). Source parameters of moderate size earthquakes and the importance of receiver crustal structure in interpreting observations of local earthquakes, *Bull. Seism. Soc. Am.* **67,** 301–313.
Kanamori, H. and D. L. Anderson (1975). Theoretical basis of some empirical relations to seismology, *Bull. Seism. Soc. Am.* **65,** 1073–1095.
Kanamori, H. and G. S. Stewart (1976). Mode of the strain release along the Gibbs fracture zone, Mid-Atlantic ridge, *Phys. Earth Planet. Interiors* **11,** 312–332.
Kim, S. G. and O. W. Nuttli (1977). Spectral and magnitude characteristics of anomalous Eurasian earthquakes, *Bull. Seism. Soc. Am.* **67,** 463–478.
Langston, C. A. (1976). A body wave inversion of the Koyna, India earthquake of 10 December 1967 and some implication for body wave focal mechanisms, *J. Geophys. Res.* **81,** 2517–2529.
Langston, C. A. and R. Butler (1976). Focal mechanism of the August 1, 1975 Oroville earthquake, *Bull. Seism. Soc. Am.* **66,** 1111–1120.
Langston, C. A. and D. V. Helmberger (1975). A procedure for modeling shallow dislocation sources, *Geophys. J.* **42,** 117–130.
Madariaga, R. (1976). Dynamics of an expanding circular fault, *Bull. Seism. Soc. Am.* **66,** 639–666.
Mendiguren, J. A. (1971). Focal mechanism of a shock in the middle of the Nazca plate, *J. Geophys. Res.* **76,** 3861–3879.
Nogochi, S. and K. Abe (1977). Earthquake source mechanism and $M_s - m_b$ relation, *J. Seism. Soc. Japan* **30,** 487–507.
Richardson, R. M. (1978). Finite element modeling of stress in the Nazca plate: driving forces and plate boundary earthquakes, *Tectonophysics* **50,** 223–248.
Richardson, R. M., S. C. Solomon, and N. H. Sleep (1976). Intraplate stresses as an indicator of plate tectonic driving forces, *J. Geophys. Res.* **81,** 1847–1856.
Richardson, R. M. and S. C. Solomon (1977). Apparent stress and stress drop for intraplate earthquakes and tectonic stress in the plates, *Pageoph* **115,** 317–331.
Richardson, R. M., S. C. Solomon, and N. H. Sleep (1978). Tectonic stress in the plates (submitted for publication).
Stein, S. (1978). An earthquake swarm on the Chagos-Laccadive ridge and its tectonic implications, *Geophys. J.* **55,** 577–588.
Stein, S. (1979). Intraplate seismicity on bathymetric features: the 1968 Emperor Trough earthquake, *J. Geophys. Res.* **84,** 4763–4768.
Stein, S. and E. A. Okal (1978). Seismicity and tectonics of the Ninetyeast Ridge area: evidence for internal deformation of the Indian Plate, *J. Geophys. Res.* **83,** 2233–2246.
Sykes, L. R. (1970). Focal mechanism solutions for earthquakes along the world rift system, *Bull. Seism. Soc. Am.* **60,** 1749–1752.
Sykes, L. R. (1978). Intraplate seismicity reactivation of pre-existing zones of weakness, alkaline magmatism and other tectonism post-dating continental fragmentation, *Rev. Geophys. Space Phys.* **16,** 621–688.
Sykes, L. R. and M. L. Sbar (1973). Intraplate earthquakes, lithospheric stresses and the driving mechanism of plate tectonics, *Nature* **245,** 298–302.
Sykes, L. R. and M. L. Sbar (1974). Focal mechanism solutions of intraplate earthquakes and stresses in the lithosphere, Kristjansson, Editor, *Geodynamics of Iceland and the North Atlantic Area,* 207–224.
Tatham, R. H., D. W. Forsyth, and L. R. Sykes (1976). The occurrence of anomalous seismic events in

eastern Tibet, *Geophys. J.* **45,** 451–481.
Wang, S. C., R. J. Geller, S. Stein, and B. Taylor (1979). An intraplate thrust earthquake in the South China Sea, *J. Geophys. Res.* **84,** 5627–5632.

SEISMOLOGICAL LABORATORY
DIVISION OF GEOLOGICAL AND PLANETARY SCIENCES
CALIFORNIA INSTITUTE OF TECHNOLOGY
PASADENA, CALIFORNIA 91125
CONTRIBUTION NO. 3364

Manuscript received March 19, 1980